7-1-2014

The regulator of G protein signaling (RGS) domain of G protein-coupled receptor kinase 5 (GRK5) regulates plasma membrane localization and function.

Hua Xu
Department of Biochemistry and Molecular Biology, Thomas Jefferson University

Xiaoshan Jiang
Department of Biochemistry and Molecular Biology, Thomas Jefferson University; Center for Science Research, Guilin Medical University

Ke Shen
Center for Science Research, Guilin Medical University

Christopher C. Fischer
Department of Biochemistry and Molecular Biology, Thomas Jefferson University, Christopher.Fischer@jefferson.edu

Philip B Wedegaertner
Department of Biochemistry and Molecular Biology, Thomas Jefferson University, Philip.Wedegaertner@jefferson.edu

The regulator of G protein signaling (RGS) domain of G protein–coupled receptor kinase 5 (GRK5) regulates plasma membrane localization and function

Hua Xu[a,*], Xiaoshan Jiang[a,b,*], Ke Shen[b], Christopher C. Fischer[a], and Philip B. Wedegaertner[a]
[a]Department of Biochemistry and Molecular Biology, Thomas Jefferson University, Philadelphia, PA 19107; [b]Center for Science Research, Guilin Medical University, Guilin, Guangxi 541004, China

ABSTRACT **The G protein–coupled receptor (GPCR) kinases (GRKs) phosphorylate activated GPCRs at the plasma membrane (PM). Here GRK5/GRK4 chimeras and point mutations in GRK5 identify a short sequence within the regulator of G protein signaling (RGS) domain in GRK5 that is critical for GRK5 PM localization. This region of the RGS domain of GRK5 coincides with a region of GRK6 and GRK1 shown to form a hydrophobic dimeric interface (HDI) in crystal structures. Coimmunoprecipitation (coIP) and acceptor photobleaching fluorescence resonance energy transfer assays show that expressed GRK5 self-associates in cells, whereas GRK5-M165E/F166E (GRK5-EE), containing hydrophilic mutations in the HDI region of the RGS domain, displays greatly decreased coIP interactions. Both forcing dimerization of GRK5-EE, via fusion to leucine zipper motifs, and appending an extra C-terminal membrane-binding region to GRK5-EE (GRK5-EE-CT) recover PM localization. In addition, GRK5-EE displays a decreased ability to inhibit PAR1-induced calcium release compared with GRK5 wild type (wt). In contrast, PM-localized GRK5-EE-CaaX (appending a C-terminal prenylation and polybasic motif from K-ras) or GRK5-EE-CT shows comparable ability to GRK5 wt to inhibit PAR1-induced calcium release. The results suggest a novel model in which GRK5 dimerization is important for its plasma membrane localization and function.**

Monitoring Editor
Josephine C. Adams
University of Bristol

Received: Sep 23, 2013
Revised: Apr 25, 2014
Accepted: Apr 25, 2014

INTRODUCTION

The G protein–coupled receptor (GPCR) kinases (GRKs) specifically phosphorylate agonist-activated GPCRs at the cytoplasmic surface of the plasma membrane (PM). Phosphorylated GPCRs uncouple the heterotrimeric G proteins and recruit arrestins to form receptor/arrestin complexes that undergo endocytosis, resulting in GPCR degradation or recycling back to the PM. GRK-regulated desensitization of GPCR signaling can thus prevent an excessive cellular response to receptor activation and provides a necessary turn-off mechanism to regulate GPCR signaling in response to variable stimuli.

Seven GRK family members can be divided into three subgroups based on their amino acid identity: GRK1 and 7; GRK2 and 3; and GRK4–6. GRK1 and 7 are specifically expressed in the retina. The other GRKs are ubiquitously expressed, except for GRK4, which is mostly restricted to testes, brain, and kidney. All GRKs share similar architecture. After a short N-terminal region, GRKs have a regulator of G protein signaling (RGS) domain, a catalytic kinase domain, and a variable C-terminal region (Gurevich *et al.*, 2012).

To phosphorylate activated GPCRs in a timely manner, GRKs need to localize to the cytoplasmic surface of the PM. The mechanisms used by GRKs to bind membranes remain to be fully elucidated, but it is clear that GRK C-termini play prominent roles. Of

This article was published online ahead of print in MBoC in Press (http://www.molbiolcell.org/cgi/doi/10.1091/mbc.E13-09-0547) on May 7, 2014.

*These authors contributed equally to this work.

Address correspondence to: Xiaoshan Jiang (jiangxs@glmc.edu.cn), Philip Wedegaertner (philip.wedegaertner@jefferson.edu).

Abbreviations used: DSP, dithiobis[succinimidylpropionate]; GPCR, G protein–coupled receptor; GRK, GPCR kinase; HDI, hydrophobic dimeric interface; HEK293, human embryonic kidney; PM, plasma membrane; RGS, regulator of G protein signaling.

Supplemental Material can be found at:
http://www.molbiolcell.org/molbiolcell/suppl/2014/05/05/mbc.E13-09-0547v1.DC1.html

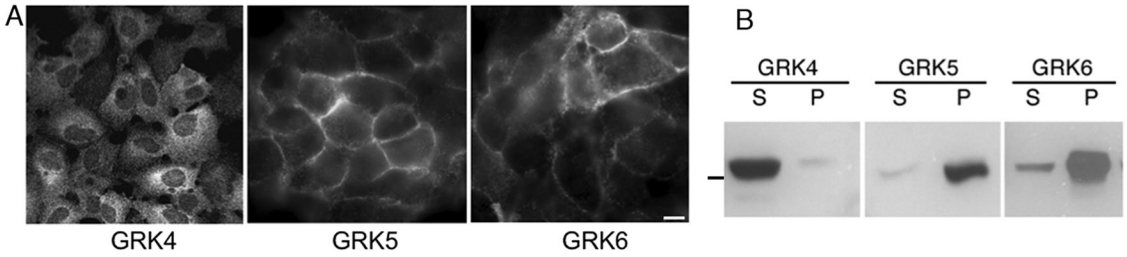

FIGURE 1: Subcellular localization of GRK4–6. (A) HEK293 cells stably expressing GRK4, 5 or 6, as indicated, were subjected to immunofluorescence staining using a GRK4–6 antibody that detects all three GRKs. Bar, 10 μm. (B) HEK293 cells stably expressing GRK4, 5, or 6 were lysed, and the cell lysates were fractionated by high-speed centrifugation into soluble (S) and particulate (P) fractions, as described in *Materials and Methods*. GRKs were detected by immunoblotting with a GRK4–6 antibody. The black bar indicates a 70-kDa standard. Images and immunoblots shown are representative from at least three experiments.

interest, the C-terminal regions of the different GRK subfamilies are quite diverse in terms of sequence and structure and indeed have been shown to use unique mechanisms to promote GRK PM localization (Gurevich *et al.*, 2012). GRK1 and 7 rely on a carboxyl-terminal CaaX motif that promotes covalent modification by a farnesyl or geranylgeranyl isoprenoid (Inglese *et al.*, 1992); these hydrophobic lipids are well known to serve as membrane anchors. In contrast, GRK2 and 3 each contains a pleckstrin homology (PH) domain in the C-terminal region that mediates translocation of the kinases from the cytoplasm to the PM upon GPCR activation (Pitcher *et al.*, 1992; Barak *et al.*, 1999; Carman *et al.*, 2000). The PH domain allows GRK2 and 3 to anchor on the PM by interacting with both phospholipids and free G protein βγ subunits. Finally, GRK4–6 all have a predicted C-terminal amphipathic helix motif defined by a hydrophobic helix core surrounded by several basic residues (Pronin *et al.*, 1998; Thiyagarajan *et al.*, 2004; Jiang *et al.*, 2007). GRK5 and 6 appear to localize constitutively at the PM in cells, but subcelluar localization of GRK4 has not been well addressed. In addition to the amphipathic helix, GRK4 and 6 can be palmitoylated on C-terminal cysteines (Stoffel *et al.*, 1994; Premont *et al.*, 1996; Loudon and Benovic, 1997; Vatter *et al.*, 2005; Jiang *et al.*, 2007). The covalent attachment of palmitate appears to be necessary, together with the amphipathic helix, for PM localization of GRK6 (Jiang *et al.*, 2007), but the role of the amphipathic helix and palmitoylation in GRK4 remains to be examined.

To identify additional mechanisms that regulate PM localization of GRK5, we compared the localization of GRK4–6 and then focused on GRK5 in these studies. Surprisingly, whereas expressed GRK5 and 6 are localized on the PM, expressed GRK4 is found predominantly in the cytoplasm. Using GRK5/4 chimeras and point mutations in GRK5, we identify amino acids in the RGS domain of GRK5 that are necessary for PM localization. These amino acids map to a region in GRK6 and 1 determined in crystal structures to mediate a hydrophobic dimeric interface (HDI), and, consequently, we show that expressed GRK5 can exist in a complex in cells. This study suggests a novel mechanism in which amino acids in the RGS domain of GRK5 regulate its PM localization by mediating a dimeric interaction.

RESULTS

GRK5/4 chimeras reveal a novel protein region involved in PM localization of GRK5

Previous work demonstrated the importance of an amphipathic helix in the C-terminal extension of GRK5 and 6 for PM localization, and for GRK6, palmitoylation in the C-terminal extension is also required (Stoffel *et al.*, 1994, 1998; Loudon and Benovic, 1997; Pronin *et al.*, 1998; Thiyagarajan *et al.*, 2004; Vatter *et al.*, 2005; Jiang *et al.*, 2007). Although not yet tested for subcellular localization, the C-terminus of GRK4α (hereafter referred to as GRK4) likewise contains a predicted amphipathic helix and sites for palmitoylation (Premont *et al.*, 1996; Pronin *et al.*, 1998; Thiyagarajan *et al.*, 2004). However, when stably expressed in human embryonic kidney (HEK293) cells, immunofluorescence microscopy demonstrated that GRK4 was distributed throughout the cytoplasm, in contrast to the strong PM localization of GRK5 and 6 (Figure 1A). Consistent with the immunofluorescence analysis, separation of cell lysates by high-speed centrifugation into soluble/cytosol (S) or particulate/membrane (P) fractions revealed that GRK4 was found almost exclusively in the soluble fraction, whereas GRK5 and 6 were predominantly found in the particulate fraction (Figure 1B). These results indicate an unexpected difference in subcellular localization among the members of this subfamily of GRKs.

To identify the basis for this difference, we focused on a comparison of PM-localized GRK5 and cytoplasmic GRK4, and we first tested whether differences in their C-termini could explain the dramatic difference in subcellular localization. GRK5 remains at the PM when its C-terminus is replaced by that of GRK4 (Figure 2), indicating that the C-terminus of GRK4 has sufficient PM targeting information to compensate for the loss of GRK5's C-terminus. Moreover, GRK4 remains in the cytoplasm when its C-terminus is replaced by that of GRK5 (Figure 2); thus, although the C-terminus of GRK5 is required for GRK5 PM localization, it is not sufficient to promote PM localization of GRK4. Taken together, these results show that C-terminal differences are not responsible for the different subcellular localization of GRK5 and 4 and suggest that protein regions in addition to the C-terminus play a critical role in regulating PM localization of this GRK family.

Therefore we reasoned that additional GRK5/4 chimeras would identify novel determinants of PM localization (Figure 2A). We focused on the RGS domains because they contained the least sequence identity in GRK5 versus GRK4. Replacing amino acids 95–134 in the RGS domain of GRK5 with amino acids 95–134 of GRK4 did not affect localization; this GRK5/4RGS(95–134) chimera remained localized at the PM similar to wt GRK5 (Figure 2). On the other hand, a GRK5/4RGS(135–170) chimera, in which amino acids 135–169 of GRK5 were replaced with amino acids 135–170 of GRK4, was localized in the cytoplasm (Figure 2). Thus a critical and novel determinant for membrane localization of GRK5 appears to be contained within amino acids 135–169 of its RGS domain. Further mutagenesis showed that chimera GRK5/4RGS(165–169), which simply

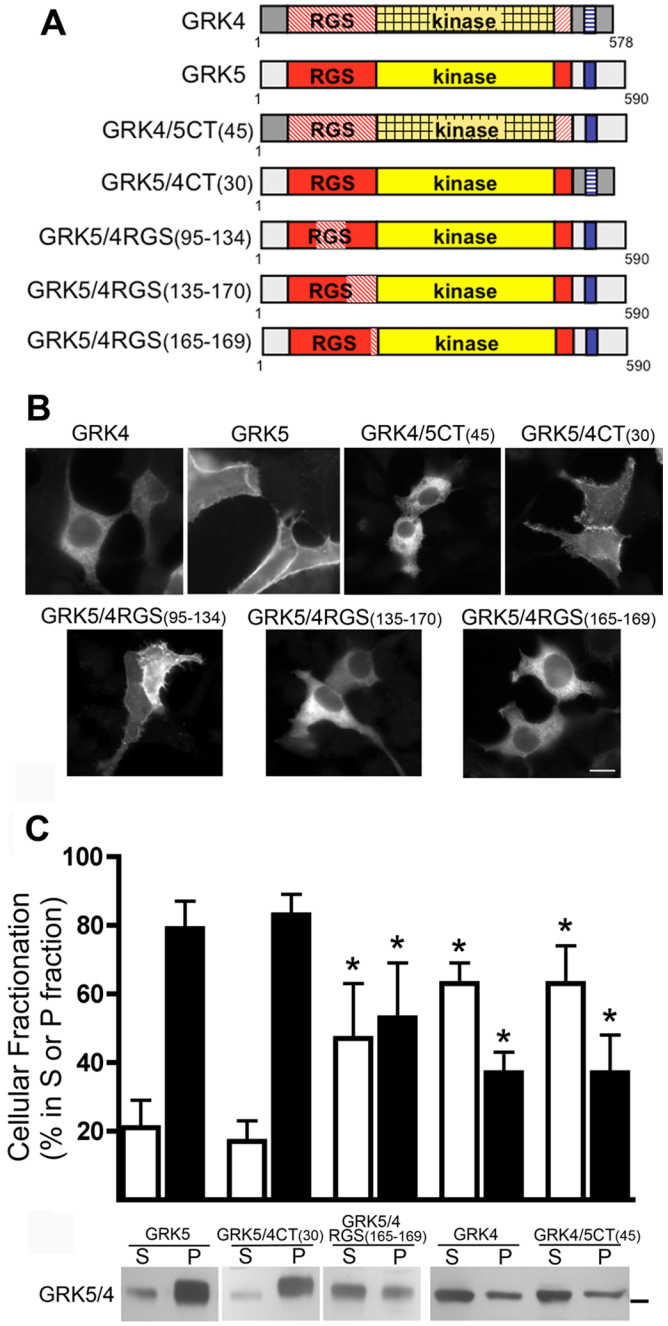

FIGURE 2: GRK5/4 chimeras identify a region of the RGS domain as a novel determinant of PM localization of GRK5. (A) Schematic representations of GRK chimeras. In GRK4/5CT(45), the C-terminus of GRK4 (amino acids 548–577) is replaced with the C-terminus of GRK5 (amino acids 546–590). Conversely, in GRK5/4CT(30), the C-terminus of GRK5 (amino acids 546–590) is replaced with that of GRK4 (amino acids 548–577). Chimera GRK5/4RGS(95–134) was generated by replacing a region of the RGS domain (amino acids 95–134) of GRK5 with the corresponding region of the GRK4 RGS domain (amino acids 95–134). Chimera GRK5/4RGS(135–170) was generated by replacing a second part of the RGS domain (amino acids 135–169) of GRK5 with the corresponding region of the GRK4 RGS domain (amino acids 135–170). Chimera GRK5/4RGS(165–169) was generated by replacing amino acids 165–169 of GRK5 with the amino counterparts from GRK4, resulting in the four amino substitutions M165S/F166Y/D168S/R169Q in GRK5. (B) Plasmids expressing the indicated chimeras of GRK5 and 4 were transiently transfected into HEK293 cells. Immunofluorescence microscopy was performed using the GRK4–6 antibody as described in *Materials and Methods*. Images shown are representative from at least three experiments. Bar, 10 μm. (C) Plasmids expressing the indicated chimeras of GRK5 were transiently transfected into HEK293 cells, and subcellular fractionation into soluble (S) and particulate (P) fractions was performed, as described in *Materials and Methods*. GRK5 and 4 constructs were detected after immunoblotting with a GRK4–6 monoclonal antibody or a GRK4 polyclonal antibody, respectively. The black bar indicates a 70-kDa standard. The graph shows quantitation (average ± SD, $n \geq 3$) of gel bands of S and P fractions from multiple experiments. Statistical analysis was performed using one-way analysis of variance ($p < 0.05$) to indicate significant difference among all the groups, followed by *t*-test comparison between any of the two groups. Asterisks indicate statistical significance ($p < 0.05$) of the indicated S fraction vs. the GRK5 S fraction or of the indicated P fraction vs. the GRK5 P fraction.

replaces four GRK5 amino acids within 165–169 with their GRK4 amino acid counterparts (M165S/F166Y/D168S/R169Q), was sufficient to shift localization of GRK5 into the cytoplasm and soluble fraction (Figure 2).

A novel determinant of PM localization of GRK5 maps to a hydrophobic dimeric interface

Strikingly, the region of the RGS domain identified in the foregoing contains part of a conserved HDI identified in crystal structures of GRK6 and 1 (Lodowski *et al.*, 2006; Singh *et al.*, 2008; Boguth *et al.*, 2010; Tesmer *et al.*, 2012). The HDI in the crystal structure of GRK6 is composed of key hydrophobic residues I39, I165, Y166, and F527. In GRK5, amino acids at the corresponding positions are I39, M165, F166, and F527; the similarity of these key residues in GRK5 and 6 suggests that GRK5 would also contain an HDI (Figure 3A and Supplemental Figure S1). Note that M165 and F166 are found within the RGS domain region identified in Figure 2 as being critical for PM localization of GRK5; in the GRK5/4RGS(135–170) and GRK5/4RGS(165–169) chimeras, which show loss of PM localization, M165 is replaced with a serine, along with other amino acid substitutions.

To test more directly whether the HDI region of the RGS domain plays a role in regulating GRK5 PM localization, we mutated three key HDI-forming hydrophobic residues, M165, F166, and F527, to negatively charged D or E in order to disrupt the ability of these side chain to mediate hydrophobic interactions. Similar mutations to negatively charged amino acids were shown to not affect the kinase activity of GRK6 (Lodowski *et al.*, 2006). Single mutants M165E, F166E, and F527D and double mutants M165E/F166E (EE) and M165E/F527D (ED) were expressed in HEK293 cells, and subcellular localization was assayed by immunofluorescence microscopy and subcellular fractionation. Of interest, all mutants showed much reduced PM localization compared with wt GRK5 (Figure 3B and Supplemental Figure S2); the double mutants displayed prominent localization in the cytoplasm, whereas the single mutants showed strong cytoplasmic localization with a retention of some PM staining. Fractionation analyses showed a decrease of membrane localization for all GRK5 mutants (Figure 3C). Double mutant GRK5-EE showed the highest loss of membrane binding; >65% of GRK5-EE was found in the soluble fraction (Figure 3C). To examine the possibility that the introduction of the negatively charged glutamic acids was preventing PM localization of GRK5 by decreasing binding to negatively charged membrane phospholipids, we generated two additional mutants. Both the neutral GRK5-M165A/F166A mutant and the positive-charge GRK5-M165K/F166K mutant showed loss of PM localization and membrane fractionation identical to GRK5-EE

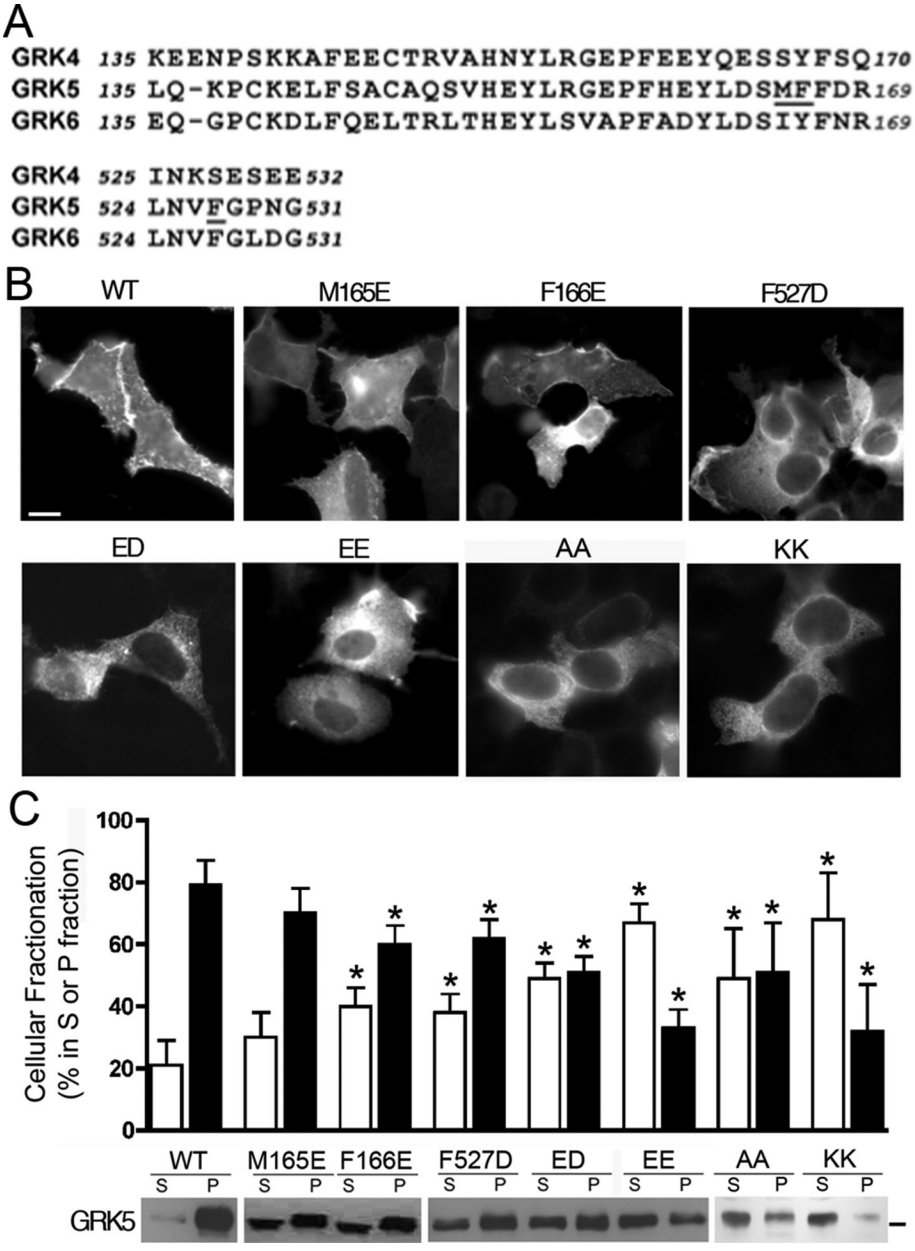

FIGURE 3: A hydrophobic dimeric interface within the RGS domain is a novel determinant for GRK5 PM targeting. (A) The region of the RGS domain of GRK5 identified in the GRK5/4RGS(135–170) chimera is aligned with the same region of GRK4 and GRK6 (top alignment), and a short region at the end of helix 11 of the RGS domains of GRK4–6 is also aligned (bottom alignment). Key amino acids that are mutated here in GRK5 and that correspond to amino acids that form important hydrophobic interactions in the dimeric structure of GRK6 are underlined. (B) Plasmids expressing the following HDI mutants of GRK5 were transiently transfected into HEK293 cells: GRK5 (wt), GRK5-M165E (M165E), GRK5-F166E (F166E), GRK5-F527D (F527D), GRK5-M165E/F166E (EE), GRK5-M165E/F527D (ED), GRK5-M165A/F166A (AA), and GRK5-M165K/F166K (KK). Immunofluorescence microscopy was performed using the GRK4–6 antibody as described in *Materials and Methods*. Shown are images of one to three cells under a 60× objective. Images shown are representative images from at least three experiments. Bar, 10 μm. (C) Plasmids expressing the indicated HDI mutants of GRK5 were transiently transfected into HEK293 cells, and subcellular fractionation into soluble (S) and particulate (P) fractions was performed, as described in *Materials and Methods*. GRK5 was detected after immunoblotting with a GRK4–6 antibody. The graph shows quantitation (average ± SD, $n \geq 3$) of gel bands of S and P fractions from multiple experiments. Statistical analysis was performed using one way analysis of variance ($p < 0.05$) to indicate significant difference among all the groups, followed by *t*-test comparison between any of the two groups. Asterisks indicate statistical significance ($p < 0.05$) of the indicated S fraction vs. the wt S fraction or of the indicated P fraction vs. the wt P fraction.

(Figure 3, B and C), arguing against a specific role for the amino acid side chain's charge in disrupting PM localization of GRK5. Taken together, these results show that disruption of key hydrophobic residues in the GRK5 HDI domain significantly impaired the PM targeting of GRK5, suggesting that this HDI domain contributes to GRK5 PM localization.

HDI-mediated complex formation of GRK5 in cells

GRK6 and GRK1 exist as HDI-mediated dimers in multiple crystal structures (Lodowski *et al.*, 2006; Singh *et al.*, 2008; Boguth *et al.*, 2010; Tesmer *et al.*, 2012). Although the structure of GRK5 has not been reported, it is predicted, based on sequence similarity, to contain a similar HDI domain capable of mediating its homodimerization (Figure 3A and Supplemental Figure S1). However, it was reported that the purified, palmitoylation-deficient mutant of GRK6 was a monomer in solution (Lodowski *et al.*, 2006), as was a nonfarnesylated, soluble form of GRK1 (Singh *et al.*, 2008), and purified, soluble GRK5 also behaves as a monomer in solution (J. Benovic, personal communication). Nonetheless, the authors speculated that GRK6 and 1 may physiologically dimerize inside cells in the presence of membranes and interacting proteins (Lodowski *et al.*, 2006; Singh *et al.*, 2008; Tesmer *et al.*, 2012). The lack of dimer detection of soluble GRK1, 5, or 6 suggests that if self-association occurs in cells, it may be weak and thus difficult to detect. Keeping this in mind, we sought to examine whether GRK5 can form complexes in cells.

First, we examined complex formation by coimmunoprecipitation. Because numerous attempts to coimmunoprecipitate different tagged forms of GRK5 from cell lysates failed to provide reliable results, we used a cell-permeable cross-linker to attempt to trap GRK5 protein complexes before cell lysis. GRK5 tagged with S and hemagglutinin (HA) epitopes, respectively, were expressed in HEK293 cells, and, after treatment of the cells with the cross-linker dithiobis[succinimidylpropionate] (DSP), cell lysates were subjected to an affinity precipitation assay to pull down S-tagged GRK5 (GRK5-S) using S-protein-agarose. In the precipitate, HA-tagged GRK5 (GRK5-HA) was detected by immunoblotting, suggesting an interaction of the two tagged forms of GRK5 (Figure 4A). Identical pull-down assays with HDI-disrupted GRK5-EE revealed a lack of GRK5-EE-S and GRK5-EE-HA coprecipitation, suggesting that GRK5 dimerization is dependent on its HDI. To rule out the trivial explanation

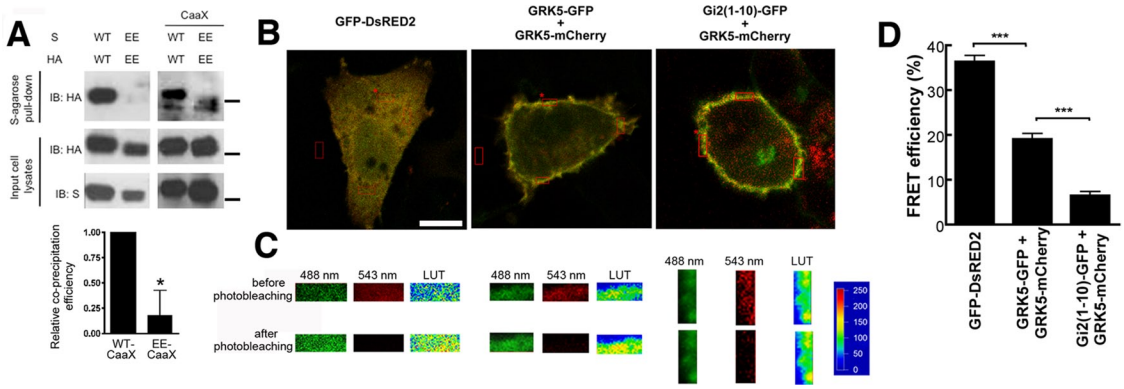

FIGURE 4: HDI-mediated self association of GRK5. (A) Pairs of S and HA epitope–tagged forms of GRK5, GRK5-EE, GRK5-CaaX, or GRK5-EE-CaaX were transiently coexpressed in HEK293 cells as indicated. Cells were treated with the cell-permeable cross-linker DSP, cells were then lysed, and affinity precipitation was performed with S-agarose beads. The S-agarose pull down was immunoblotted with an HA antibody to detect coprecipitation of the two tagged forms of GRK5 (top), and cell lysates were immunoblotted with HA antibody (middle) or S antibody (bottom). Immunoblots shown are representative from at least three experiments. The black bars indicate a 70-kDa standard. The graph shows quantitation (average ± SD, $n = 3$) of relative coprecipitation efficiency of the S- and HA-tagged forms of GRK5-EE-CaaX (EE-CaaX) vs. the S- and HA-tagged forms of GRK5-CaaX (wt-CaaX). Quantitation of the pull-down gel bands of GRK5-EE-CaaX and GRK5-CaaX (top) were normalized by the input cell lysate (middle). The asterisk indicates statistical significance (*t* test, $p < 0.05$) of the relative coprecipitation efficiency of GRK5-EE-CaaX vs. GRK5-CaaX. (B–D) HEK293 cells were transfected with the indicated pairs of plasmids. As described in *Materials and Methods*, cells were imaged by confocal microscopy. Merged images of the GFP and mCherry channels are shown. Bar, 10 μm. Regions of interest as shown by the red rectangles in B were analyzed by acceptor photobleaching FRET. Fluorescence changes in the GFP channel were determined before and after acceptor photobleaching of mCherry (50-s application of 543-nm wavelength) in regions of interest (asterisk in B indicates the region of interest shown in C). (D) The FRET efficiency of GRK5-GFP + GRK5-mCherry calculated from $E = (I_D - I_{DA})/I_D$, where I_D is the peak in the presence of the sensitized acceptor and I_{DA} is the peak of donor (GFP) emission in the presence of the acceptor. The Gi2(1-10)-GFP + GRK5-mCherry pair was used as negative and the GFP-DsRed as positive control for protein–protein interaction, respectively. Each bar represents mean ± SEM of FRET efficiency, using six cells with three regions of interest per cell ($n = 18$). Statistical analysis was performed using *t*-test comparison between groups. Asterisks (***) indicate statistical significance ($p < 0.0001$). Similar results were obtained in three experiments.

that GRK5-EE is not detected in a complex in this assay due to its localization in the cytoplasm rather than the PM, we generated PM-localized forms of GRK5-EE by appending a C-terminal CaaX motif from K-Ras. Although strongly targeted to the PM (Supplemental Figure S3), S- and HA-tagged forms of GRK5-EE-CaaX were greatly reduced in their ability to coprecipitate compared with tagged forms of GRK5 or GRK5-CaaX (Figure 4A). Similarly, appending an additional C-terminus rescues PM localization of GRK5-EE (described later in Figure 6) but does not promote coprecipitation (Supplemental Figure S4). Thus lack of PM localization does not explain the inability of GRK5-EE to coprecipitate in this assay. Instead, our results using cross-linking followed by coprecipitation are consistent with GRK5 forming dimers or higher-order complexes in cells, and mutation at the HDI disrupts this interaction.

In addition, we examined GRK5 complex formation using acceptor photobleaching fluorescence resonance energy transfer (FRET; Figure 4, B–D). GRK5–green fluorescent protein (GFP) and GRK5-mCherry were coexpressed in HEK293 cells and, as expected, colocalized on the PM (Figure 4B). On photobleaching the GRK5-mCherry fluorescence in a region of interest at the PM, the GRK5-GFP fluorescence was enhanced, indicating close association of GRK5-GFP and GRK5-mCherry (Figure 4, C and D). A positive control in which GFP and the red fluorescent protein DsRed2 are linked in a single fusion protein gave a strong FRET signal (Figure 4, B–D). To control for FRET that is simply a consequence of colocalization at the PM rather than a protein–protein interaction, GFP was targeted to the PM by virtue of fusion to the first 10 amino acids of the G protein α_{i2} and was coexpressed with GRK5-mCherry (Figure 4B). Much-reduced FRET was observed by the acceptor photobleaching approach in cells expressing $G\alpha_{i2}$-GFP and GRK5-mCherry (Figure 4, C and D), suggesting that the observed GRK5-GFP/GRK5-mCherry interaction is not simply due to colocalization at the PM. Taken together, the different experimental approaches in Figure 4 provide evidence for GRK5 self-association in transfected cells.

Forced dimerization of GRK5-EE rescues its impaired PM targeting

We showed that disruption of the HDI in GRK5-EE resulted in decreased GRK5 complex formation and significant loss of GRK5 PM localization (Figures 3 and 4), suggesting a model in which GRK5 dimerization is critical for its PM localization. Thus we hypothesized that inducing dimerization of GRK5-EE would promote relocalization of GRK5-EE to the PM. To test this prediction, we appended strongly dimerizing leucine zipper motifs derived from the transcription factors Jun (JLZ) and Fos (FLZ; O'Shea *et al.*, 1989; Patel *et al.*, 1996; Rieker and Hu, 2000; Stuhlmann-Laeisz *et al.*, 2006) to GRK5-EE and GRK5. JLZ-GRK5-EE and FLZ-GRK5-EE coimmunoprecipitated after expression in HEK293 cells, consistent with the ability of the attached leucine zipper motifs to promote dimerization (Figure 5C). Of importance, immunofluorescence microcopy in HEK293 cells showed that leucine zipper–mediated GRK5-EE dimers (JLZ-GRK5-EE and FLZ-GRK5-EE) were relocalized on the PM compared with cytoplasmic GRK5-EE (Figure 5A). Fractionation analysis of JLZ-GRK5-EE and FLZ-GRK5-EE also demonstrated significant increase in membrane

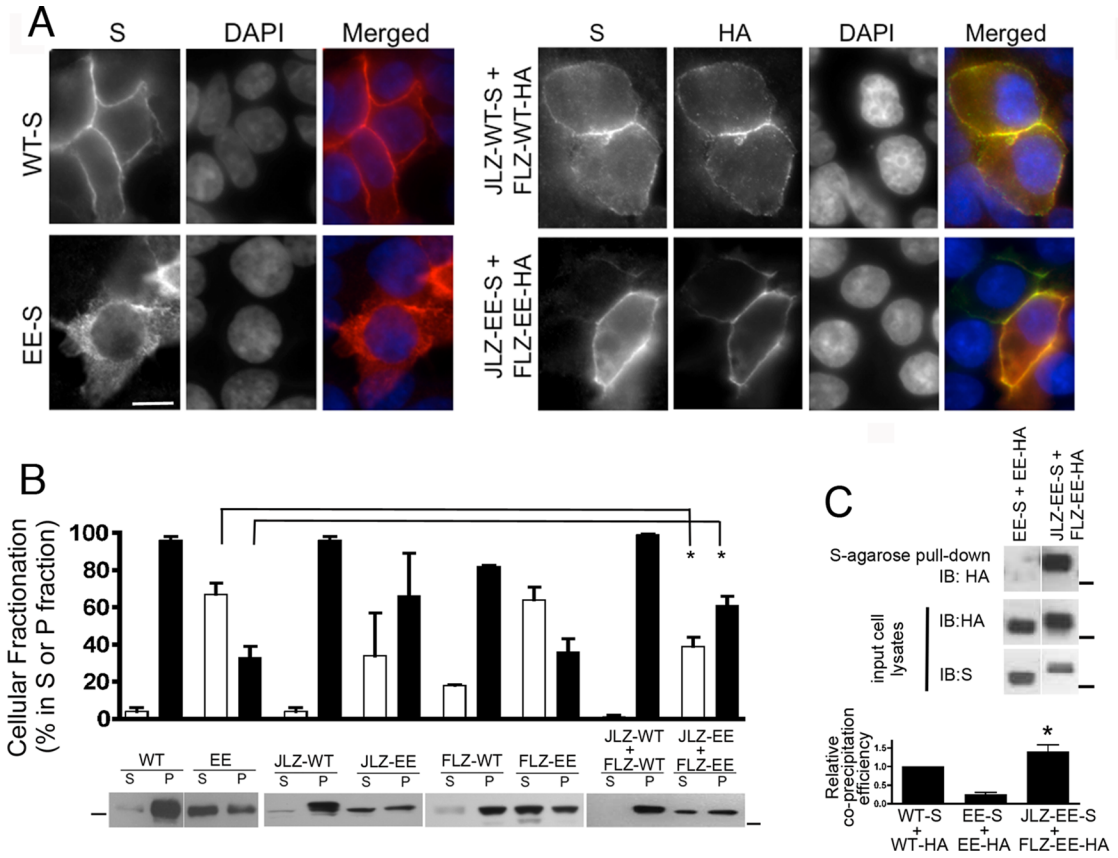

FIGURE 5: Leucine zipper–mediated dimerization of GRK5-EE rescues PM localization. (A) HEK293 cells were transiently transfected with plasmids expressing S-tagged GRK5, S-tagged GRK5-EE, and S-tagged JLZ-GRK5 together with HA-tagged FLZ-GRK5, or S-tagged JLZ-GRK5-EE together with HA-tagged FLZ-GRK5-EE. Immunofluorescence microscopy was performed using a mouse monoclonal anti-S antibody followed by Alexa 594–conjugated secondary antibody and a rabbit polyclonal anti-HA antibody followed by Alexa 448–conjugated secondary antibody. Nuclei were stained with DAPI. Images shown are representative from at least three experiments. Bar, 10 μm. (B) HEK293 cells were transiently transfected with the indicated constructs as described in A. Subcellular fractionation into soluble (S) and particulate (P) fractions was performed, and samples were immunoblotted with a mouse monoclonal anti–GRK4–6 antibody. The black bars indicate a 70-kDa standard; the one on the left corresponds to lanes 1–4, and the one on the right corresponds to the remaining lanes. The graph shows quantitation (average ± SD, $n \geq 3$, except $n = 2$ for JLZ-wt, JLZ-EE, FLZ-wt, and FLZ-EE) of gel bands of S and P fractions from multiple experiments. Statistical analysis was performed using one way analysis of variance ($p < 0.05$) to indicate significant difference among all the groups, followed by *t*-test comparison between any of the two groups. Asterisks indicate key statistical significance ($p < 0.05$) of the indicated S fraction vs. the EE S fraction or of the indicated P fraction vs. the EE P fraction. (C) Pairs of S and HA epitope–tagged forms of GRK5-EE or the S-tagged JLZ-GRK5-EE and HA-tagged FLZ-GRK5-EE pair were transiently coexpressed in HEK293 cells as indicated. Cells were treated with the cell-permeable cross-linker DSP, cells were then lysed, and affinity precipitation was performed with S-agarose beads. The S-agarose pull down was immunoblotted with an HA antibody to detect coprecipitation of the two tagged forms of GRK5 (top), and cell lysates were immunoblotted with HA antibody (middle) or S antibody (bottom). Each row is from the same immunoblot at the same film exposure; intervening, irrelevant lanes were simply removed. The black bars indicate a 70-kDa standard. The graph shows quantitation (average ± SEM, $n = 3$) of relative coprecipitation efficiency of the S- and HA-tagged forms of the indicated GRK5 mutants. Quantitation of the pull-down gel bands (top) were normalized by the input cell lysate (middle). The asterisk indicates statistical significance (*t* test, $p < 0.05$) of the relative coprecipitation efficiency of the S-tagged JLZ-GRK5-EE and HA-tagged FLZ-GRK5-EE pair vs. the S-tagged GRK5-EE and HA-tagged GRK5-EE pair.

partitioning compared with that of GRK5-EE (Figure 5B), suggesting that GRK5 dimerization is essential for its PM localization.

Tandem C-termini rescue PM localization of GRK5-EE

Our model predicts that monomeric GRK5 binds weakly to membranes inside cells, but dimerization allows bivalent or multivalent interactions with membranes and thus strong membrane binding. Thus we tested this idea by appending an extra C-terminal region (residues 546–590), containing the amphipathic helix region required for membrane binding, to the HDI-domain mutant GRK5-EE and testing for rescue of PM localization. GRK5-EE-CT containing such a tandem C-terminus localized prominently at the PM, as opposed to the cytoplasmic localization of GRK5-EE (Figure 6A), showing a striking shift to being predominantly in the membrane fraction upon fractionation of cell lysates (Figure 6B). These results are consistent with a model in which dimerization of GRK5 allows membrane-binding domains from two molecules of GRK5 to contribute to PM localization.

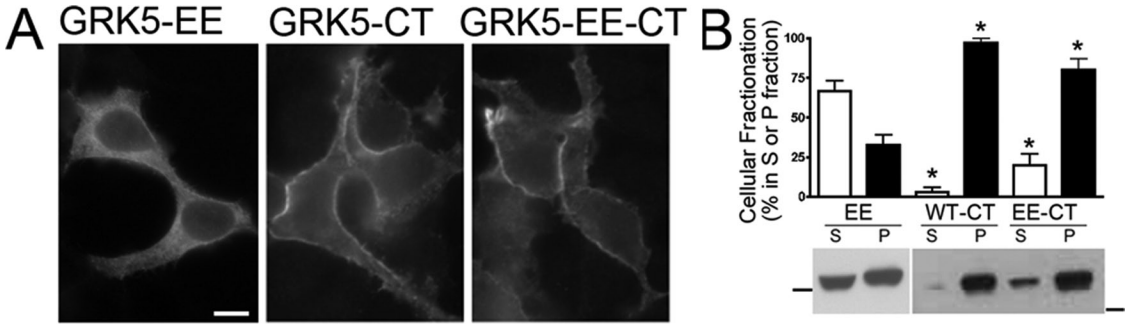

FIGURE 6: Tandem C-termini promote PM localization of GRK5-EE. (A) Plasmids expressing GRK5-EE, S-tagged GRK5-CT, or S-tagged GRK5-EE-CT were transiently transfected into HEK293 cells. Immunofluorescence microscopy was performed using a mouse monoclonal anti–GRK4–6 antibody or the mouse monoclonal anti-S antibody as described in *Materials and Methods*. Images shown are representative from at least three experiments. Bar, 10 μm. (B) Plasmids expressing GRK5-EE, S-tagged GRK5-CT, or S-tagged GRK5-EE-CT were transiently transfected into HEK293 cells. Subcellular fractionation into soluble (S) and particulate (P) fractions was performed, and samples were immunoblotted with a mouse monoclonal anti–GRK4–6 antibody or the mouse monoclonal anti-S antibody. The black bars indicate a 70-kDa standard; the one on the left corresponds to lanes 1 and 2, and the one on the right corresponds to the remaining lanes. The graph shows quantitation (average ± SD, $n = 3$) of gel bands of S and P fractions from multiple experiments. Statistical analysis was performed using one-way analysis of variance ($p < 0.05$) to indicate significant difference among all the groups, followed by *t*-test comparison between any of the two groups. Asterisks indicate statistical significance ($p < 0.01$) of the indicated S fraction vs. the EE S fraction or of the indicated P fraction vs. the EE P fraction.

Decreased cellular function of GRK5-EE is rescued by forced PM localization

Previous work demonstrated that HDI mutations in GRK1 and GRK6 had little or no effect on phosphorylation of rhodopsin in vitro, suggesting that the HDI domain does not regulate the intrinsic kinase activity of GRKs (Lodowski *et al.*, 2006; Singh *et al.*, 2008). Thus we predicted that GRK5-EE would have decreased ability in cells to regulate GPCR function due to its decreased PM localization. To test this, we assayed the ability of expressed GRK5 to decrease Ca^{2+} signaling by the protease-activated receptor 1 (PAR1), an established target of GRK5 (Tiruppathi *et al.*, 2000). Addition of thrombin agonist peptide to HEK293 cells results in robust Ca^{2+} signaling, but transient or stable overexpression of GRK5 reduces the Ca^{2+} response to 30–40% of that of cells transfected with empty vector (Figure 7, A and B). In contrast, in HEK293 cells transiently or stably overexpressing PM localization-deficient GRK5-EE, Ca^{2+} release upon activation of PAR1 was 70% of that of control cells (Figure 7, A and B). As a comparison, GRK5-4A, containing mutations of the four key hydrophobic residues in the C-terminal amphipathic helix membrane-binding region (Thiyagarajan *et al.*, 2004), is likewise deficient in inhibiting PAR1-mediated Ca^{2+} signaling (~80% of control) compared with wt GRK5 (Figure 7A), consistent with decreased localization at the PM. When HEK293 cells were transiently transfected with PM-bound GRK5-EE-CT or GRK5-EE-CaaX, PAR1-mediated Ca^{2+} signaling was inhibited in a manner similar to that seen with GRK5 (Figure 7, C and D), showing that restoration of PM localization can recover the decreased function of GRK5-EE.

DISCUSSION

This article demonstrates a key role for a surface of the RGS domain of GRK5 in regulating its PM localization. The results provide evidence for a novel PM targeting mechanism in which RGS domain–mediated dimerization is necessary for PM localization of GRK5. Several lines of evidence support this. First, chimeras and site-specific mutations show that disruption of select RGS-domain amino acids results in loss of PM localization of GRK5. Moreover, these amino acids map to a surface of the RGS domain that was observed to mediate dimeric interactions in crystal structures of GRK6 and 1. Second, cross-linking coprecipitation studies and FRET show GRK5–GRK5 complex formation in transfected cells. Third, recovery of PM localization of the cytoplasmic GRK5 RGS domain mutant by forced dimerization or by appending an additional membrane-targeting C-terminal region provides further support for a model in which dimerization allows multivalent membrane binding of GRK5.

RGS domain–mediated dimerization of GRK5 is supported by recent crystal structures of GRK6 and 1 in which an extensive surface area forms an HDI. The overall structure of the RGS domain and the dimeric surface are highly similar in GRK6 and 1, and the two GRKs use very similar amino acids to form the HDI. Of importance, GRK5 is also predicted to form a similar HDI based on amino acid identity (Lodowski *et al.*, 2006; Figure 3A and Supplemental Figure S1). Of interest, dimers of purified GRK6 or 1 could not be detected in solution (Lodowski *et al.*, 2006; Singh *et al.*, 2008). However, those studies used a soluble palmitoylation-deficient mutant of GRK6 and a soluble nonfarnesylated form of GRK1. It is possible that binding to membranes facilitates the formation of dimers and that dimers could exist inside the cell in the presence of membranes and other proteins. This would suggest that dimerization of these GRKs is dynamic inside the cell. Indeed, we were initially unable to reproducibly coimmunoprecipitate different tagged forms of GRK5, suggesting that GRK5 dimers were not stable upon cell lysis, but the use of a cell-permeable cross-linker before cell lysis allowed us to capture GRK5 complexes. Of importance, mutation of M165 and F166 (GRK5-EE), two key amino acids in the predicted HDI of GRK5, disrupted complex formation in our coprecipitation assay (Figure 4A), even when GRK5-EE was localized to the PM by virtue of a CaaX motif. In addition, a report showed coimmunoprecipitation of different tagged forms of GRK5, although mutational disruption of the coimmunoprecipitated complex was not tested (Chen *et al.*, 2011). Consistent with disruption of dimerization by our mutations in GRK5, another report showed that a L166K mutation in GRK1, mapping to the same position as M165 in GRK5, resulted in the first crystal structure of GRK1 as a monomer (Tesmer *et al.*, 2012). The L166K mutation did not perturb the overall structure of GRK1; it only

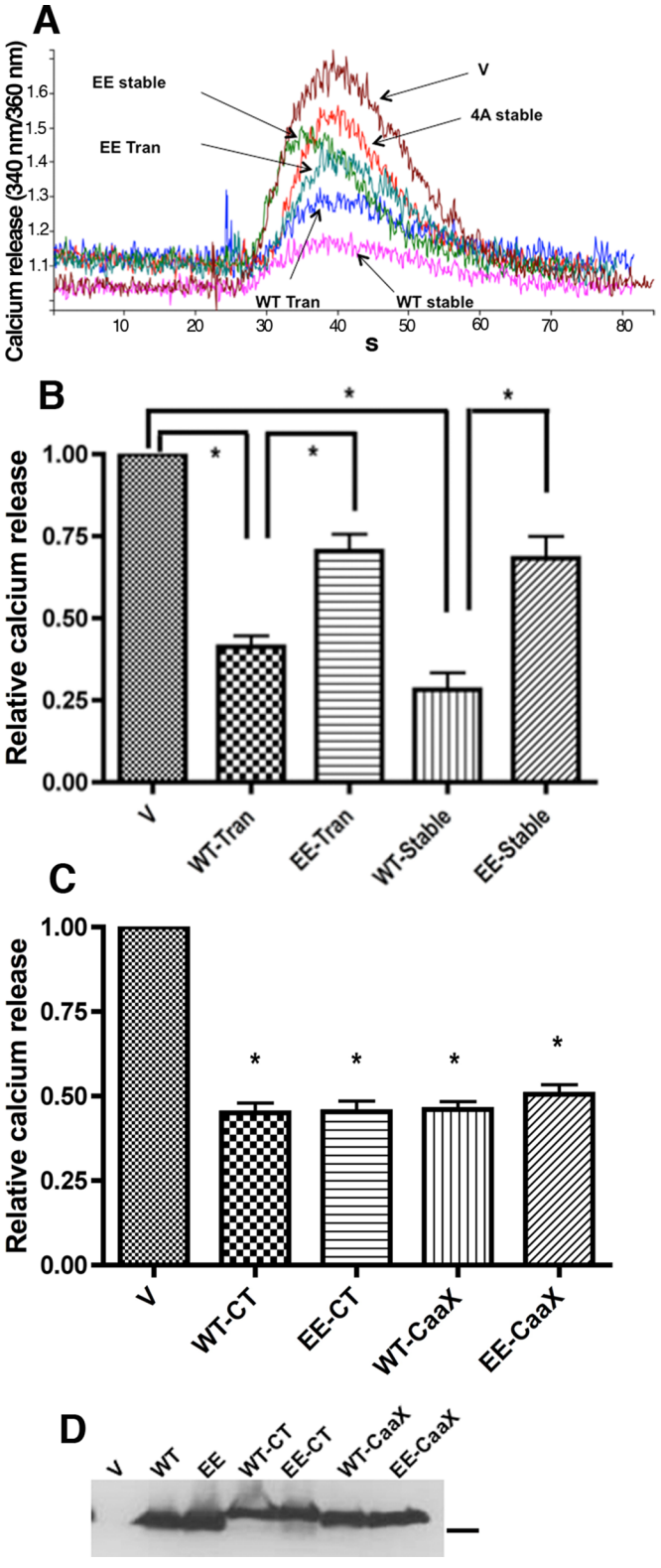

FIGURE 7: Regulation of PAR1-mediated signaling by GRK5-EE. (A) HEK293 cells were either stably or transiently transfected with vector (V), GRK5 (wt), GRK5-EE (EE), or GRK5-4A (4A) as indicated. The cells were treated with 100 nM PAR1 agonist peptide. The change of cytoplasmic calcium concentration was measured using a Fura-2 calcium mobilization assay described in *Materials and Methods*. Briefly, the calcium concentration reflected by the ratio of emission at 340/380 nm (*y*-axis) was recorded over time of stimulation (*x*-axis). The peak value (the distance between the top of the peak and baseline) of the calcium concentration curve was calculated to reflect the maximal magnitude of PAR1 signaling activation for each of the transfected samples. (B, C) PAR1 peptide agonist–stimulated calcium release was measured in HEK293 cells stably expressing GRK5 or GRK5-EE or HEK293 cells transiently expressing GRK5, GRK5-EE, GRK5-CT, GRK5-EE-CT, GRK5-CaaX, or GRK5-EE-CaaX, as indicated. The peak value of the calcium concentration in vector transfected cells was normalized as arbitrary unit 1. Statistical analysis was performed using one-way analysis of variance ($p < 0.05$) to indicate significant difference among all the groups, followed by *t*-test comparison between any of the two groups (B and C, $n = 3$). *$p < 0.05$. (D) Cell lysates from a representative experiment of transiently transfected HEK293 cells were immunoblotted using the GRK4–6 antibody. The black bar indicates a 70-kDa standard.

disrupted the ability of GRK1 to crystallize as a dimer. A key future question is whether one can detect self-association of endogenous GRKs, specifically GRK1, 5, or 6. This a very challenging question, as there exists a dearth of techniques for demonstrating homodimerization of an endogenous nontagged protein.

In addition to suggesting that GRK5 dimerizes in the cell to promote PM localization, our results raise the possibility that lack of dimerization of GRK4 may be responsible for our observation that expressed GRK4 is cytoplasmic rather than localized to the PM (Figures 1 and 2). Although RGS domain sequence comparisons indicate that GRK2 and 3 do not have an HDI, all other GRKs were predicted to have a similar HDI capable of mediating dimerization (Lodowski *et al.*, 2006). However, our GRK5/4 chimeras indicate important differences in the two RGS domains in terms of promoting PM localization, and closer inspection of the RGS sequence identifies key amino acid differences that might prevent formation of a HDI in GRK4. Specifically, GRK6 and 1 dimerize in crystal structures using a central interdigitated aromatic stack and additional hydrophobic interactions composed of amino acids I39/I165/Y166/F527 and L44/L166/Y167/W531, respectively, and GRK5 has a similar predicted hydrophobic core consisting of I39/M165/F166/F527. However, the amino acids at the similar positions in GRK4 are V39/S166/Y167/S528. The presence of S166 rather than a hydrophobic isoleucine, leucine, or methionine and the presence of S528 rather than the hydrophobic phenylalanine or tryptophan would be predicted to prevent the formation of an HDI in GRK4. Thus we speculate that the observed cytoplasmic localization of GRK4 (Figures 1 and 2) reflects an inability of GRK4 to dimerize, and, moreover, we predict that introduction of an HDI into GRK4 would promote its PM localization. Initial attempts to test this idea by generating GRK4/GRK5 chimeras failed to relocalize GRK4 to the PM. Certainly, it is easier to generate loss-of-function/localization than gain-of-function/localization mutants, and the mechanism behind the localization differences of GRK5 and 4 remain to be understood.

One functional role for dimerization of GRK5 appears to be simply to regulate PM localization. We showed that the cytoplasmic HDI mutant GRK5-EE less efficiently reduced PAR1-mediated calcium signaling than PM-localized GRK5 wt; however, returning GRK5-EE to the PM by appending a CaaX motif or an additional GRK5 C-terminus allowed GRK5-EE to function similarly to GRK5 wt (Figure 7). Consistent with this, it is worth noting that other reports have shown that mutation of key HDI residues in GRK1, 6, and 5 do not affect kinase activity and phosphorylation of GPCRs in vitro (Lodowski *et al.*, 2006; Singh *et al.*, 2008; Baameur *et al.*, 2010). However, we cannot rule out that GRK5 dimerization has functional roles independent of regulating PM localization. In this regard, Chen *et al.* (2011) proposed that dimerization of GRK5 is necessary for a novel role of

GRK5 in actin bundling. Future studies will be needed to fully define the role of the HDI region of the RGS domain in GRK5 function.

We propose a refined model for the mechanisms that regulate PM localization of GRK5. Previous work showed that the C-terminal region of GRK5 was a critical determinant of PM localization, and our previous studies predicted that a C-terminal amphipathic helix was crucial (Pronin *et al.*, 1998; Thiyagarajan *et al.*, 2004; Jiang *et al.*, 2007). The C-terminal amphipathic helix, which is also present in GRK4 and GRK6, is proposed to bind membranes through a central patch of hydrophobic amino acid side chains and also by surrounding basic amino acids that would interact with acidic membrane lipid headgroups. In addition, GRK5 can interact with membranes via an N-terminal basic region shown to bind phosphatidylinositol 4,5-bisphosphate (PIP2; Pitcher *et al.*, 1996; Chen *et al.*, 2011). Whether the N-terminal PIP2-binding motif directs PM localization or modulates membrane domain localization and kinase activity once GRK5 is localized to the PM remains to be clearly defined. Nonetheless, it is clear that multiple regions of GRK5 can contribute to PM localization. However, our results predict that such membrane-binding regions promote only weak membrane localization of monomeric GRK5 inside the cell. Consequently, dimerization of GRK5 would allow multivalent and therefore strong membrane binding. Consistent with this idea, our previous work showed that whereas the C-terminal amphipathic helix region of GRK5 was necessary for PM localization, when fused to GFP it only promoted partial PM localization, suggesting that the C-terminus is a weak membrane-targeting signal (Thiyagarajan *et al.*, 2004). Following from this idea, in this study PM localization of cytoplasmic GRK5-EE was recovered when an additional C-terminus was fused to it. We propose that in the absence of RGS domain–mediated dimerization, the additional C-terminus mimicked the multivalent membrane binding that would be promoted by GRK5 dimerization. Such dimerization-facilitated strong membrane localization has been observed in other proteins. For example, dimerization has been shown to be necessary for phosphatidylinositol 3-phosphate–binding FYVE domains to promote strong localization to endosomal membranes (Hayakawa *et al.*, 2004; Cho and Stahelin, 2005).

Taken together, previous work and our results here suggest a novel model in which dimerization of GRK5 is critical for PM localization. Regulation of the ability of GRK5 to dimerize would provide a point of regulation of GRK5's localization and function inside the cell. Moreover, the development of an inhibitor to disrupt GRK5 self-association, and thus PM localization and function, may provide a way to specifically target GRK5 in disease.

MATERIALS AND METHODS

Cell culture

HEK293 cells were cultured in DMEM supplemented with 10% fetal bovine serum (FBS) and 1% penicillin and streptomycin. All cell lines were incubated in a 5% CO_2 atmosphere at 37°C.

Constructs

The full-length human GRK5 in pcDNA3 construct was provided by Jeffrey Benovic (Thomas Jefferson University, Philadelphia, PA; Kunapuli and Benovic, 1993). Human GRK4α was generously provided by Richard Premont (Duke University, Durham, NC) and was subcloned into pcDNA3. Single or double mutations of the RGS domain, as well as the quadruple mutant GRK5/4RGS(165–169), were generated using QuikChange (Stratagene) site-directed mutagenesis. S tag (KETAAAKFERQHMDS) or HA tag (YPYDVPDYA) was fused at the carboxy terminus of GRK5 constructs. To generate leucine zipper constructs, the nucleotide fragments of the Jun leucine zipper (JLZ) motif (RIARLEEKVKTLKAQNSELASTANML-REQVAQLKQKVMN) and the Fos leucine zipper (FLZ) motif (LT-DTLQAETDQLEDEKSALQTEIANLLKEKEKLEFILAA) were amplified by PCR. Following an initiating methionine, each motif sequence was appended to the N-terminal end of GRK5 by a peptide linker (GGSGGGSGGGSG). Tandem C-termini constructs were generated by linking a GRK5 C-terminal region (amino acids 546–590) to the C-terminal end of full-length GRK5 following a peptide linker (DSAGSAG). To make GRK5 CaaX constructs, a K-Ras4B CaaX tail (GKKKKKKSKTKCVIM) was directly appended downstream of the S or HA tags of GRK5 constructs. All the constructs were cloned into pcDNA3.1 or pcDNA3 vector.

Plasmid transfection

For transient transfection, cells were seeded at 40–50% confluency in cell culture dishes overnight. Plasmids were mixed with Lipofectamine 2000 reagent (Invitrogen, Grand Island, NY) at reagent-to-DNA ratio of 3:1 according to manufacturer's protocol. The mixture was placed in the cell dishes, and the cells were incubated for 48 h before further analysis. The stable line of GRK5-expressing HEK293 cells was also generated for this study. Briefly, GRK5 plasmids were transfected into HEK293 cells, and positive clones were screened in the presence of G418.

Immunofluorescence microscopy

Cells were fixed in 3.7% formaldehyde on coverslips for 15 min, followed by incubation in TBS solution supplemented with 1% Triton X-100 (TBS-Triton) and 2.5% milk for blocking for 20 min. Then cells were incubated with primary antibodies (mouse monoclonal anti-S tag [Novagen, Darmstadt, Germany], rabbit polyclonal anti-HA tag [Santa Cruz, Biotechnology, Dallas, TX], and mouse monoclonal anti-GRK4-6 [Millipore, Darmstadt, Germany]) at dilution of 1:1000 (for all the primary antibodies used) in TBS-Triton solution with 2.5% milk for 1 h at room temperature, followed by five washes with TBS-Triton solution with 2.5% milk. Cells were then incubated with anti-mouse and anti-rabbit secondary antibodies preconjugated with Alexa 488 or Alexa 594 (Invitrogen) at dilution of 1:100 (for both secondary antibodies) in TBS-Triton solution with 2.5% milk for 30 min at room temperature, followed by five washes with TBS-Triton solution. The nuclei were stained with 4′,6-diamidino-2-phenylindole (DAPI). Coverslips were mounted to glass slides in Prolong Gold antifade mounting medium (Invitrogen) overnight. Images were recorded with an Olympus BX-61 microscope (Olympus, Melville, NY) and 60× planApo objective with an ORCA-ER (Hamamatsu, Bridgewater, NJ) cooled charge-coupled device camera controlled by SlideBook, version 4.0 (Intelligent Imaging Innovation, Denver, CO). Images were transferred to Photoshop (Adobe, San Jose, CA) for digital processing.

Quantitation of single cells was performed after deconvolution. Image stacks were deconvolved using a constrained iterative algorithm in SlideBook, version 4.0, and images of *xy*-planes through the middle of cells were used for analysis. Quantitation of deconvolved images of single cells was performed using the Plot Profile tool of ImageJ (National Institutes of Health, Bethesda, MD). The relative magnitude GRK5 distribution along a linear slice of the cell was quantitated, similar to that described previously (Thiyagarajan *et al.*, 2002; Irannejad *et al.*, 2013). The pixel intensity in eight or nine line scans from four or more cells for each GRK5 mutant was determined, the pixel intensity was normalized to 1, and then the average pixel intensity was plotted using Prism (GraphPad, La Jolla, CA).

Affinity pull-down assay

The transfected cells were treated with cross-linker DSP (Invitrogen) at 2 μM final concentration in phosphate-buffered saline (PBS) buffer for 30 min at room temperature according to manufacturer's protocol. The cells were then lysed in Triton lysis buffer (1% Triton X-100, 25 mM Tris-HCl, pH 7.4, 150 mM NaCl, 5% glycerol, 1 mM EDTA, 2 mM Na_3PO_4, 1 mM NaF, 20 mM $Na_4P_2O_7$) supplemented with protease inhibitor tablet (Roche, Basel, Switzerland) on ice for 15–30 min. Cell lysates were spun down at low speed, and the supernatant was collected for total protein quantification. Equivalent amounts (400–600 μg) of total protein lysate from each sample were incubated with 30 μl of S-agarose beads (Novagen) through rotation for 1–2 h at 4°C. The S-agarose beads were then washed three times with Triton lysis buffer before being mixed in sample buffer for SDS–PAGE electrophoresis.

Calcium mobilization assay

The transfected cells were detached from Petri dishes in cell stripper solution (Cellgro, Manassas, VA) and collected in 15-ml conical tubes in Hank's balanced salt solution (HBSS) buffer at 5×10^6 cells/ml. The cells were incubated with 3 μM Fura-2 (Invitrogen) in the dark for 30 min at 37°C. Then the cells were washed and resuspended in HBSS buffer supplemented with 0.025% bovine serum albumin. To induce intracellular calcium release, 2×10^6 cells of each sample in 1.6-ml volume were stimulated with PAR1 agonist peptide (SFLLRN; GenScript, Piscataway, NJ) at 100 nM. Cytoplasmic calcium concentration was measured by a fluorescence spectrometer using excitation at 340 and 380 nm according to the manufacturer's protocol. The calcium release was recorded by FL WinLab program.

Western blotting

Protein samples were mixed with sample buffer and boiled for 10 min before SDS–PAGE. The separated proteins were transferred onto a polyvinylidene fluoride membrane. The membrane was blocked for 1 h in TBST buffer supplemented with 5% milk. The protein of interest was probed with the indicated primary antibodies overnight at 4°C, followed by horseradish peroxidase–conjugated secondary antibody for 1 h at room temperature. The protein of interest was detected using an enhanced chemiluminescence reaction.

Fractionation assay

The transfected cells were scraped off the culture dishes and suspended in detergent-free hypotonic buffer (50 mM Tris-HCl, pH 8, 2.5 mM $MgCl_2$, 1 mM EDTA) supplemented with protease inhibitors (Roche). Cells were pushed through a 21-gauge needle 10 times. Cell lysates were spun down at $400 \times g$ for 5 min to discard nuclei and cell debris. The supernatants were collected and subjected to ultracentrifugation at $150{,}000 \times g$ for 20 min to separate soluble/cytosol portion (S) from particulate/membrane portion (P). Identical cell equivalents from the P and S fractions were analyzed by immunoblotting. Quantity One software (Bio-Rad, Hercules, CA) and ImageJ were used to scan films from three independent experiments and quantitate S and P immunoblot bands. Immunoblotting with HSP90 and Na/K ATPase antibodies shows that this method effectively separates cytosol and membranes, respectively (unpublished data).

Acceptor photobleaching fluorescence resonance energy transfer

HEK293 cells cultured in Falcon six-well plates (Becton Dickinson, Franklin Lakes, NJ) were transfected with 2 μg of 1) a plasmid pair of pEGFP(N1)-GRK5 and pmCherry(N1)-GRK5, 2) a plasmid pair of pEGFP(N1)-Gi2(1-10) and pmCherry(N1)-GRK5, or 3) a control plasmid pEGFP(N1)-DsRed2, respectively. Twenty-four hours after transfection, cells were replated (3×10^5 cells/well) onto coverslips. Twenty-four hours after replating, cells were fixed in 3.7% formaldehyde in PBS for 20 min at room temperature, washed with PBS, and mounted onto slides. For the acceptor photobleaching FRET, a 63× magnification/1.4 numerical aperture oil immersion objective was used with the pinhole for visualization, and images were obtained by placing the slide onto a stage in a Zeiss LSM710 confocal microscope (Carl Zeiss, Jena, Germany). Three regions of each cell were acceptor-photobleached. The 488-nm laser line was used for imaging GFP, and the 543-nm laser line was used for the acceptor-photobleaching. FRET efficiency (E) was calculated from the GFP channel images according to $E = (I_D - I_{DA})/I_D$, where I_D is the peak in the presence of the sensitized acceptor and I_{DA} is the peak of donor emission in the presence of the acceptor. Before and after the bleaching of mCherry, GFP images were collected to assess changes in donor fluorescence. To ensure similar expression levels when comparing the two sample sets GRK5-GFP/GRK5-mCh and Gi(1-10)-GFP/GRK5-mCh, cells for analysis were used for which 1) GFP and mCh intensities were similar between the two sample sets and 2) the mCh/GFP intensity ratios were similar between the two sample sets.

Statistical analysis

All the statistical analyses were performed using Prism. $p < 0.05$ was considered statistically significant.

ACKNOWLEDGMENTS

We thank Jeffrey Benovic for helpful advice and critical reading of the manuscript; Ning Tang for assistance with FRET experiments; John Pascal for assistance with GRK5 molecular modeling: Jiansong Luo for assistance with calcium assays; and Terry Hébert, Douglas Tilley, and Nevin Lambert and their laboratories for experimental help. This work was supported by National Institutes of Health Grant R01 GM56444 to P.B.W. and National Natural Sciences Foundation of China Grant 31160241 to X.J.

REFERENCES

Baameur F, Morgan DH, Yao H, Tran TM, Hammitt RA, Sabui S, McMurray JS, Lichtarge O, Clark RB (2010). Role for the regulator of G-protein signaling homology domain of G protein-coupled receptor kinases 5 and 6 in beta 2-adrenergic receptor and rhodopsin phosphorylation. Mol Pharmacol 77, 405–415.

Barak LS, Warabi K, Feng X, Caron MG, Kwatra MM (1999). Real-time visualization of the cellular redistribution of G protein-coupled receptor kinase 2 and beta-arrestin 2 during homologous desensitization of the substance P receptor. J Biol Chem 274, 7565–7569.

Boguth CA, Singh P, Huang CC, Tesmer JJ (2010). Molecular basis for activation of G protein-coupled receptor kinases. EMBO J 29, 3249–3259.

Carman CV, Barak LS, Chen C, Liu-Chen LY, Onorato JJ, Kennedy SP, Caron MG, Benovic JL (2000). Mutational analysis of Gbetagamma and phospholipid interaction with G protein-coupled receptor kinase 2. J Biol Chem 275, 10443–10452.

Chen Y, Wang F, Long H, Wu Z, Ma L (2011). GRK5 promotes F-actin bundling and targets bundles to membrane structures to control neuronal morphogenesis. J Cell Biol 194, 905–920.

Cho W, Stahelin RV (2005). Membrane-protein interactions in cell signaling and membrane trafficking. Annu Rev Biophys Biomol Struct 34, 119–151.

Gurevich EV, Tesmer JJ, Mushegian A, Gurevich VV (2012). G protein-coupled receptor kinases: more than just kinases and not only for GPCRs. Pharmacol Ther 133, 40–69.

Hayakawa A, Hayes SJ, Lawe DC, Sudharshan E, Tuft R, Fogarty K, Lambright D, Corvera S (2004). Structural basis for endosomal targeting by FYVE domains. J Biol Chem 279, 5958–5966.

Inglese J, Koch WJ, Caron MG, Lefkowitz RJ (1992). Isoprenylation in regulation of signal transduction by G-protein-coupled receptor kinases. Nature 359, 147–150.
Irannejad R *et al*. (2013). Conformational biosensors reveal GPCR signalling from endosomes. Nature 495, 534–538.
Jiang X, Benovic JL, Wedegaertner PB (2007). Plasma membrane and nuclear localization of G protein coupled receptor kinase 6A. Mol Biol Cell 18, 2960–2969.
Kunapuli P, Benovic JL (1993). Cloning and expression of GRK5: a member of the G protein-coupled receptor kinase family. Proc Natl Acad Sci USA 90, 5588–5592.
Lodowski DT, Tesmer VM, Benovic JL, Tesmer JJ (2006). The structure of G protein-coupled receptor kinase (GRK)-6 defines a second lineage of GRKs. J Biol Chem 281, 16785–16793.
Loudon RP, Benovic JL (1997). Altered activity of palmitoylation-deficient and isoprenylated forms of the G protein-coupled receptor kinase GRK6. J Biol Chem 272, 27422–27427.
O'Shea EK, Rutkowski R, Stafford WF 3rd, Kim PS (1989). Preferential heterodimer formation by isolated leucine zippers from fos and jun. Science 245, 646–648.
Patel N, Herrman JM, Timans JC, Kastelein RA (1996). Functional replacement of cytokine receptor extracellular domains by leucine zippers. J Biol Chem 271, 30386–30391.
Pitcher JA, Fredericks ZL, Stone WC, Premont RT, Stoffel RH, Koch WJ, Lefkowitz RJ (1996). Phosphatidylinositol 4,5-bisphosphate (PIP2)-enhanced G protein-coupled receptor kinase (GRK) activity. Location, structure, and regulation of the PIP2 binding site distinguishes the GRK subfamilies. J Biol Chem 271, 24907–24913.
Pitcher JA, Inglese J, Higgins JB, Arriza JL, Casey PJ, Kim C, Benovic JL, Kwatra MM, Caron MG, Lefkowitz RJ (1992). Role of βγ subunits of G proteins in targeting the β-adrenergic receptor kinase to membrane-bound receptors. Science 257, 1264–1267.
Premont RT, Macrae AD, Stoffel RH, Chung N, Pitcher JA, Ambrose C, Inglese J, MacDonald ME, Lefkowitz RJ (1996). Characterization of the G protein-coupled receptor kinase GRK4. Identification of four splice variants. J Biol Chem 271, 6403–6410.
Pronin AN, Carman CV, Benovic JL (1998). Structure-function analysis of G protein-coupled receptor kinase-5. Role of the carboxyl terminus in kinase regulation. J Biol Chem 273, 31510–31518.
Rieker JD, Hu JC (2000). Molecular applications of fusions to leucine zippers. Methods Enzymol 328, 282–296.
Singh P, Wang B, Maeda T, Palczewski K, Tesmer JJ (2008). Structures of rhodopsin kinase in different ligand states reveal key elements involved in G protein-coupled receptor kinase activation. J Biol Chem 283, 14053–14062.
Stoffel RH, Inglese J, Macrae AD, Lefkowitz RJ, Premont RT (1998). Palmitoylation increases the kinase activity of the G protein-coupled receptor kinase, GRK6. Biochemistry 37, 16053–16059.
Stoffel RH, Randall RR, Premont RT, Lefkowitz RJ, Inglese J (1994). Palmitoylation of G protein-coupled receptor kinase, GRK6. Lipid modification diversity in the GRK family. J Biol Chem 269, 27791–27794.
Stuhlmann-Laeisz C *et al*. (2006). Forced dimerization of gp130 leads to constitutive STAT3 activation, cytokine-independent growth, and blockade of differentiation of embryonic stem cells. Mol Biol Cell 17, 2986–2995.
Tesmer JJ, Nance MR, Singh P, Lee H (2012). Structure of a monomeric variant of rhodopsin kinase at 2.5 A resolution. Acta Crystallogr Sect F Struct Biol Cryst Commun 68, 622–625.
Thiyagarajan MM, Bigras E, Van Tol HH, Hebert TE, Evanko DS, Wedegaertner PB (2002). Activation-induced subcellular redistribution of G alpha(s) is dependent upon its unique N-terminus. Biochemistry 41, 9470–9484.
Thiyagarajan MM, Stracquatanio RP, Pronin AN, Evanko DS, Benovic JL, Wedegaertner PB (2004). A predicted amphipathic helix mediates plasma membrane localization of GRK5. J Biol Chem 279, 17989–17995.
Tiruppathi C, Yan W, Sandoval R, Naqvi T, Pronin AN, Benovic JL, Malik AB (2000). G protein-coupled receptor kinase-5 regulates thrombin-activated signaling in endothelial cells. Proc Natl Acad Sci USA 97, 7440–7445.
Vatter P, Stoesser C, Samel I, Gierschik P, Moepps B (2005). The variable C-terminal extension of G-protein-coupled receptor kinase 6 constitutes an accessorial autoregulatory domain. FEBS J 272, 6039–6051.